

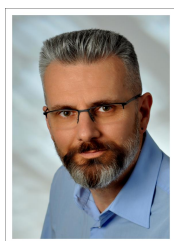


46<sup>TH</sup> TURBOMACHINERY & 33<sup>RD</sup> PUMP SYMPOSIA  
HOUSTON, TEXAS | DECEMBER 11-14, 2017  
GEORGE R. BROWN CONVENTION CENTER

## Bearing wear in electric motors and rotating equipment under the aspect of VSD converter operation

### Hans Tischmacher, Ph.D.

Senior Engineer  
Siemens AG  
Nuremberg, Germany



*Dr. Hans Tischmacher received the Dipl.-Ing. degree in electrical drives from the Technical University of Braunschweig, Germany, in 1994 and his Ph.D degree from the University of Hannover, Germany in 2017. He is currently Senior Engineer at Siemens AG, Industry Sector, Drive Technologies Division, Large Drives, Nuremberg, Germany. He has 20 years experience in the development and testing of electric motors and power electronic converters. His scientific interests include electric drive systems, power electronics, electrical machines and its application. In the last 10 years he has been working in the field of motor converter interaction, especially the side effects of the power electronic converters on electrical machines, e.g. bearing currents, noise emission, insulation stress, etc. Dr. Tischmacher is a member of the Institute of Electrical and Electronics Engineers (IEEE).*

### ABSTRACT

This paper deals with the bearing wear and the early detection of possible damages in bearings of variable-speed, converter-fed electrical motors. A description covering the issue of bearing currents in converter-fed drives along with possible countermeasures to avoid these parasitic effects is presented. However, this work focuses on the practical experiences of bearing wear influence on electric motors performance. Explicit information concerning a bearing damage due to corrugation caused by electrical currents through the bearing can only be extracted by a combined analysis of the electrical and the mechanical behavior of the bearing. For this purpose systematic measurements have to be exploited, where both the electrical measurement of bearing currents and the mechanical measurement of the bearing vibration status have to be combined for determining the bearing condition state. In addition to a description of the possibilities to determine the electrical bearing load in a drive system and the discussion of possible limit values, the focus is on the analysis of the mechanical bearing condition. A comparison between different vibration measurement methods provides a systematic approach enabling detection and classification of possible changes in bearings of the drive system i.e. motor and the attached load machine, in a very early state.

### INTRODUCTION

The number of converter-fed electrical motors is increasing steadily. The benefits of operation at variable speed and the associated advantages in the area of process control and energy efficiency is becoming more and more relevant. There is also the fact that the total costs of ownership of a variable speed drive could be at the same range or even lower in comparison to a conventional converterless motor solution due to the optimal dimensioned drive system. As a result, not only drive systems in the lower power range are using converter-fed AC motors, but also the medium to high power range up to several MW is taking advantage of them.

Apart from the advantages of converter operation, some parasitic side effects have to be considered. Particularly with the mainly employed DC link voltage source converters, there are side effects induced by the functional principle of these converters. The frequency variable voltage is generated by modulated switching of the DC link voltage of the converter. Inherently, two facts can subsequently result in parasitic reactions in the drive system: on the one hand, these are the fast voltage slopes, which are required to minimize losses in the switching devices of the converter, on the other hand, it is a common mode voltage inherently generated by the converter. Besides stressing the motor insulation system, these fast voltage slopes lead to the introduction of high frequency currents into the whole drive system, comprising converter, motor and installation grounding. As a result, insulation and air gaps act as parasitic capacitances and establish a network, in which parasitic currents can propagate accordingly. Depending on the conditions in



**46<sup>TH</sup> TURBOMACHINERY & 33<sup>RD</sup> PUMP SYMPOSIA**  
**HOUSTON, TEXAS | DECEMBER 11-14, 2017**  
**GEORGE R. BROWN CONVENTION CENTER**

the overall system, voltages across rolling bearings of the motors can occur. If these voltages exceed the breakdown field strength of the oil film, arc discharges will appear. In this way, they can induce currents in and across the anti-friction bearings of the electric motor and the attached load machine. These discharges in the lubrication gap of the affected bearings result in material alterations at the raceways of the bearings in the form of the so called corrugated patterns, resulting in an early and unplanned shutdown of the drive.

The objective is, to take measures in the overall drive system to significantly reduce these parasitic currents and thus decrease the electrical stress on the bearings. Besides the considerations regarding drive and grounding system of the installation, specifically investigations on the motor are required, particularly on the employed anti-friction bearings. The general correlations and possible countermeasures have been depicted in a number of publications and dissertations e.g. [1–6], which will be collectively described and summarized in the following paragraphs.

In order to select the best options and to take the appropriate countermeasures, it is necessary to determine – besides the electrical stress on the bearing – the mechanical condition of these rotatory element. In this paper, the required measurements that have to be conducted in the drive system and especially on the motor side are thoroughly described. In parallel, it is proven that the degree of damage of the respective bearing can be identified only by combining both electrical (current, voltage waveforms) and mechanical analysis (vibration). These analyses provide effective and practical determination of bearing degradation and the insight to define the appropriate countermeasures for bearing wear reduction.

## **BEARING DAMAGES DUE TO CURRENT PASSAGE**

As already mentioned in the introduction, parasitic currents can occur within the drive system as a result of fast switching elements in the converter. These currents can lead to damages in the bearing of electrical motors. Ahead of the description of the possible types of bearing currents with the corresponding countermeasures, the typical damage symptoms in the bearings of the drive components will be outlined. Here, the focus is on the alterations in the roller bearings. Sleeve bearings are not subject of this paper, firstly due to a more distinct separation of the sliding partners (lubrication film thickness is acc. to [7] 40 up to 50 times bigger compared to roller bearings) and secondly due to the non-existent rolling mechanism. So sleeve bearings usually have little to no abnormalities that could be traced back to an electrical stress on the bearings.

### *Characteristic damages in roller bearings due to current passage*

The arc flash, which is developing in the lubrication gap and the subsequent current flow have – among others – the following consequences [8–10]:

- (1) The energy, which is unleashed by the arc flash, results in material melt-out or vaporization in the load zone of the roller bearing. Depending on the run time, these changes can propagate over the complete circumference.
- (2) The lubricant changes its composition and the lubricity will decrease.

The meltings mentioned in (1) predominantly result in the formation of a crater-like formation with material properties that are deteriorated compared to the original condition. The hardened material is much more brittle, the underlying layer is annealed and thus softer than the basic material. These meltings (size approx. 1...5  $\mu\text{m}$ ) consolidate to a porous, spongy-like structure and lead to the typical “frosted” appearance of current-loaded raceway surfaces. In Figure 1 b the conditions are depicted macroscopically and microscopically in form of a scanning electron microscope (SEM) exposure. Generally, the frosted raceway has no influence on the lifetime of the bearing. However, the formation of ripples (“washboarding”) turns out to be much more problematic, which is characterized by a multitude of heterochromatic, gray lines, crosswise to the raceway (Figure 1 c). These lines are formed by a virtually periodic crest-and-valley structure of the raceway surface. This “washboard“ dynamically excites the rolling elements to vibrate, which results in an extremely increased wear of the bearing components. This can result in fatigue fractures and following bearing failure.

As denoted under (2), the lubricant changes its consistency and loses lubricity. The basic oil with the correspondent additives is bonded in the so-called soap frame. Due to the high temperatures, these substances are reacting: the soap frame and the basic oil are burning or coking and the additives often decompose quickly. After all, the lubricant will be discolored in black and hardened (Figure 1 a). This disintegration of the lubricant is a typical effect of damage as a result of current passage. It could decisively influence the lifetime of the lubricated roller bearings without regreasing device.



46<sup>TH</sup> TURBOMACHINERY & 33<sup>RD</sup> PUMP SYMPOSIA  
 HOUSTON, TEXAS | DECEMBER 11-14, 2017  
 GEORGE R. BROWN CONVENTION CENTER

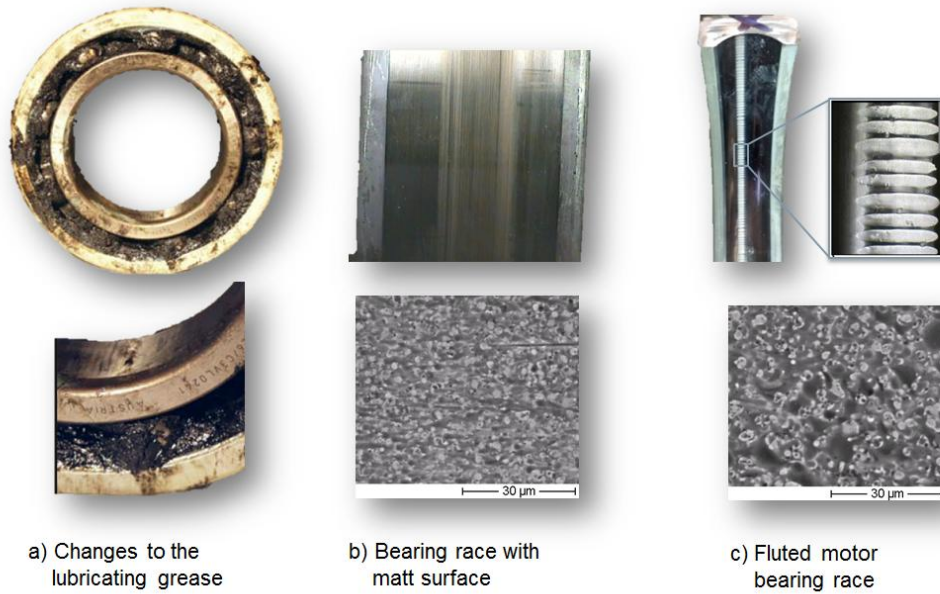


**Figure 1** Photographs of damaged motor bearings

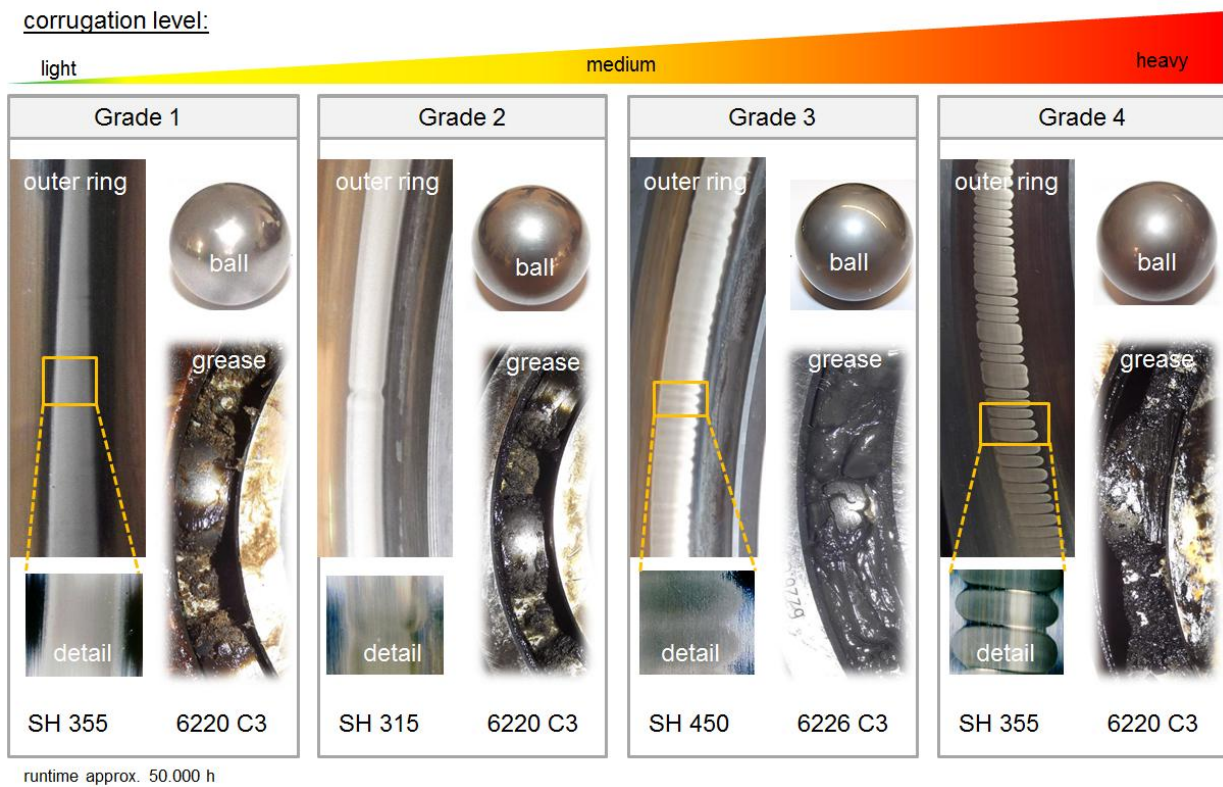


**Figure 2** Different grades of bearing damages

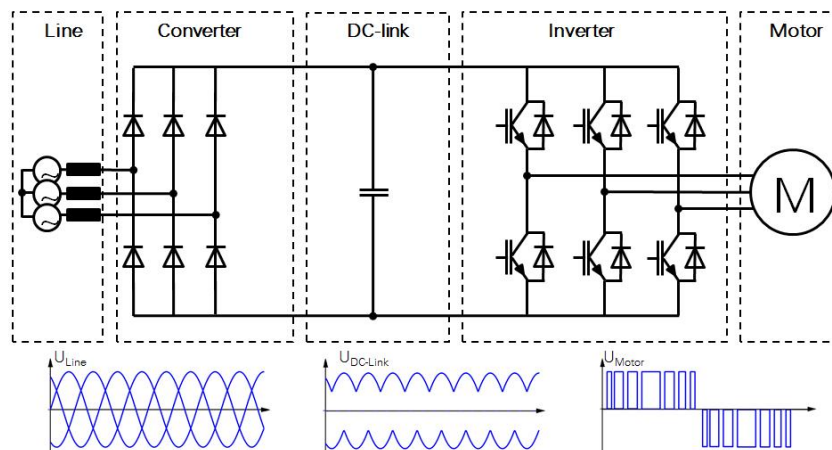


Figure 2 shows different shapes of roller bearing damages in various grades. This is based on macroscopic images of the outer raceway, the balls and the lubricants of different roller bearings, which have been operated approximately 50,000 h in motors of different shaft heights. Starting from the arising, initially slight ripple formation (Grade 1), the transition to the strong or heavy ripple formation (Grade 4) is shown in three steps. Grade 1 still shows, similar to the frosted surface depicted in Figure 1, a sequence of a multitude of small melting craters (see SEM image, Figure 1 b). Here, the frosting is an optical impression which can be attributed to a change in light scattering, induced by the summation of the melt craters. In the case of the damage of Grade 1, the first indications (shades) of an emerging crosswise ripple formation visible. In this phase, the lubricant already shows the typical black discolorations, which become perceptible with increasing degree of damage. From Grade 2 to Grade 4 an increasing crosswise ripple formation (fluting) becomes visible. Likewise, the black coloration of the grease clearly indicates the influence of an electrical bearing load.

### BEARING CURRENTS IN CONVERTER-FED DRIVE SYSTEMS

#### *Side effects of motor-converter interaction*

The converter transforms the input voltage from the supply, which is, as a first approximation, constant in amplitude and frequency, into a variable voltage in frequency and amplitude. For that purpose, a rectifier unit is feeding a DC voltage link, in which DC link capacitors act as voltage smoothers and energy storage. The subsequent inverter transforms the DC link voltage with the procedure of pulse-width modulation into a variable AC voltage. In this way, the connected electrical motor can be controlled in terms of speed and torque.



**Figure 3** Schematic diagram of a voltage source inverter (VSI)

A significant side effect in the operation of voltage source inverters (VSI) is the inherent occurrence of a common mode voltage. Due to the fact that only discrete voltages and switching states are available in a VSI, the sum of the generated phase voltages is usually non-zero - which is different to classical three-phase AC system. In addition to that, the respective modulation methods inevitably require the switching of so-called zero pointers to generate the desired output voltage. These are states of operation, where the positive or the negative DC link voltage is connected to the motor terminals. The resulting common mode voltage represents the input voltage of the described parasitic network. This means, it is - as a source - also an influencing factor for the undesired, parasitic bearing current. Metrologically, the common mode voltage represents one third of the sum of the three voltages phase-to-ground (Figure 4 at the left). In Figure 4 - at the right, the typical stepped time behavior of the common mode voltage of a two-level inverter is exemplified. Steps of  $\pm V_D/6$  and  $\pm V_D/2$  with the corresponding fast voltage changes  $dv/dt$  can be found.

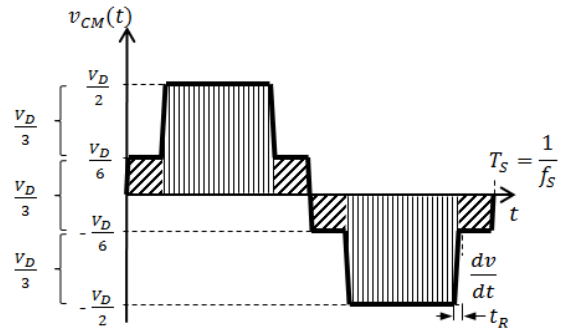
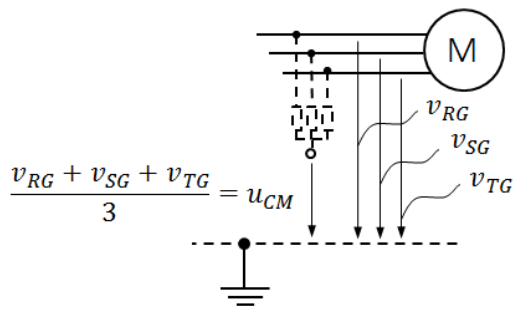


Figure 4 Definition of the common mode voltage [10]

*Bearing current types in the drive system*

The time behavior exemplified in Figure 4 represents the input variable for the parasitic network, which is established by the subsequent drive system. Because of the high-frequency signal portions, the components of this network are made up of areas, air gaps and insulation inside the drive unit, as it was already described in the introduction. The HF equivalent circuit diagram of the motor is depicted in Figure 5. Here, the common mode voltage  $v_{CM}$  induces the current component  $i_{CM}$ , which mainly flows off through the parasitic capacity component  $C_{WS}$ , which is formed between the winding system of a motor and its stator. Other capacities are present between winding and rotor ( $C_{WR}$ ), between rotor and stator ( $C_{RS}$ ) and inside the rolling bearings ( $C_B$ ). While the first three portions are determined solely by the geometric dimensions, the latter is heavily dependent on the operating conditions. Speed, temperature, bearing load and the excitation of vibrations have a very strong impact on the bearing capacity [10].

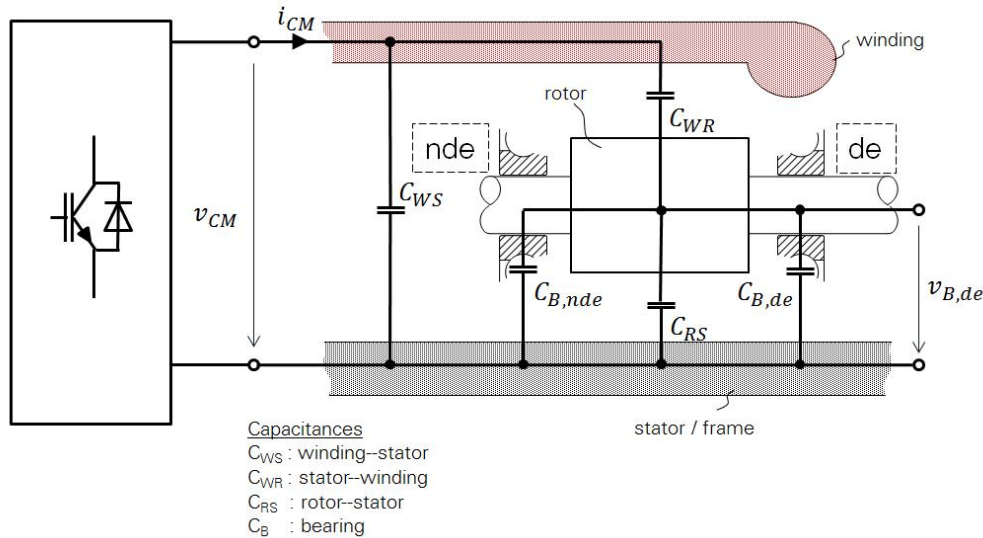


Figure 5 HF equivalent circuit diagram of a motor [10]

A distinction is made between at least three types of bearing currents: high-frequency circular currents inside the motor, EDM currents with flash-overs in the lubrication film of the bearing as well as high-frequency currents from rotor to ground. These types of bearing currents are principally shown in a schematic drive system in Figure 6. These will be explained in detail in the following paragraphs.

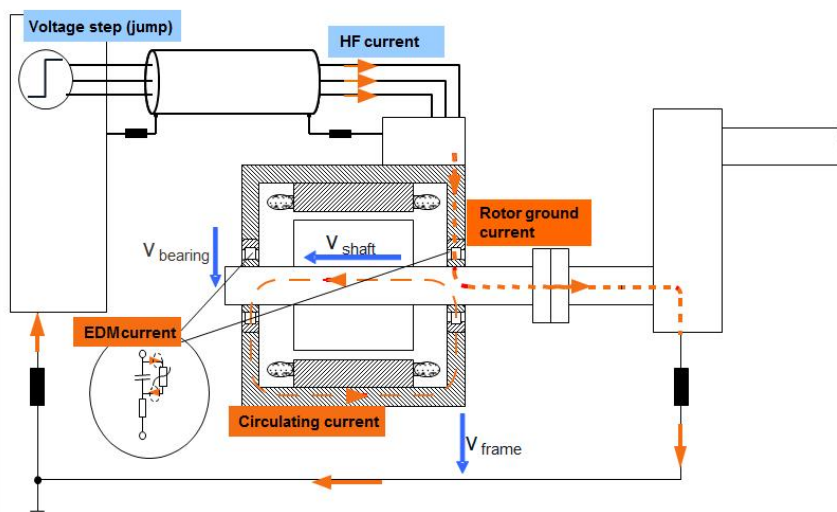


Figure 6 Bearing current types in the drive system

#### EDM currents

This type of bearing current is named according to the manufacturing process on the basis of spark erosion the so-called “Electrostatic Discharge Machining”. The basis for that is the application of the common mode voltage from the parasitic motor capacities on the lubrication gap of the rolling bearing. At this, the capacities between winding and rotor and between rotor and stator constitute a voltage divider, which generates a potential difference between rotor and stator of the motor, and thus driving a bearing current  $i_B$ . The voltage ratio can be described by the so-called “Bearing Voltage Ratio” BVR in the following equation

$$\frac{v_b}{v_{CM}} = BVR = \frac{C_{WR}}{C_{WR} + C_{RS} + 2 \cdot C_B} \quad (1)$$

In case the voltage across the bearing exceeds the breakdown voltage of the lubrication film in the bearing, the resulting arc discharge will melt or vaporize material out of the bearing raceway. In Figure 7, the waveforms of the common mode voltage, the bearing voltage at the DE bearing as well as the resulting bearing current are exemplified. It is observable that the bearing current can follow the stepped characteristic of the common mode voltage only partially, and a corresponding bearing current is measurable in the case of a voltage breakdown. The amplitude of the EDM bearing currents is depending on the amplitude of the common mode voltage of the converter, on the parasitic motor capacitances and especially on the load- and operating-point-dependent lubrication conditions in the roller bearing of the driving motor. The energy content of the arc discharge which is caused by these EDM currents is – compared to the circular currents and rotor-to-ground currents – indeed significantly smaller, but it can progressively also lead to the formation of ripples in the bearings.

There is no efficient method to avoid or at least to minimize this type of bearing current. The only conceivable countermeasure is the application of grounding brushes to short-circuit the corresponding bearing and thus avoid the development of bearing voltages. Unfortunately, this method represents only an inadequate solution, because the contact characteristics of the brush system are strongly dependent on the environmental conditions and the inherent wear requires periodic maintenance. Moreover, the application of brushes can to some extent even increase the proportions of the other type of bearing currents and therefore it must rather be considered detrimental. According to [10], the chance to at least avoid EDM bearing currents to some extent, lie particularly in the prevention of critical operating conditions, e.g. in form of an appropriate prediction of flash-over activities.

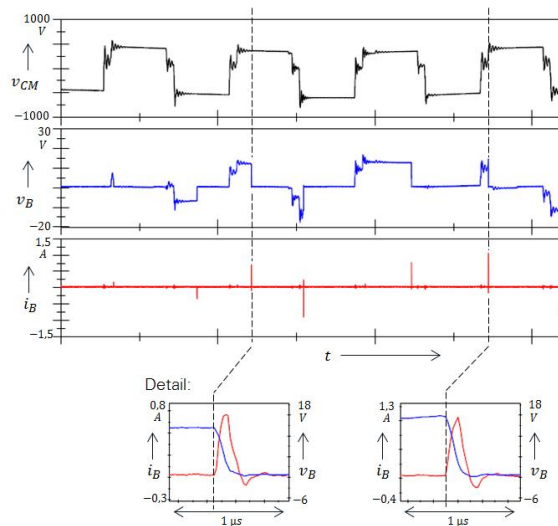


Figure 7 Example for measured EDM-current pulses [10]

*Circulating currents*

In contrast to the EDM bearing currents, the circular currents, depicted in the left part of the equivalent circuit diagram in Figure 5 has a crucial influence – in form of the parasitic capacity between winding and stator lamination  $C_{ws}$ . The high-frequency common mode current which is flowing off via the slot insulation, induces a circular magnetic flux, which encircles the shaft of the motor. The voltage induced by that flux into the shaft of the motor causes a high-frequency circular current, which closes over: laminated core – bearing shield – motor bearing – shaft. In contrast to the classical circular bearing current according to [11], which leads to a circular current with motor fundamental frequency due to magnetic unbalances. The circular current caused by converter operation features has a significantly higher frequency. The circumstances are schematically shown in Figure 8 at the left. On the right-hand side, one can find a detailed magnification of the current time plots, measured at both motor bearings. Both current courses show a phase displacement of  $180^\circ$  at identical amplitude and thus they represent a circular current.

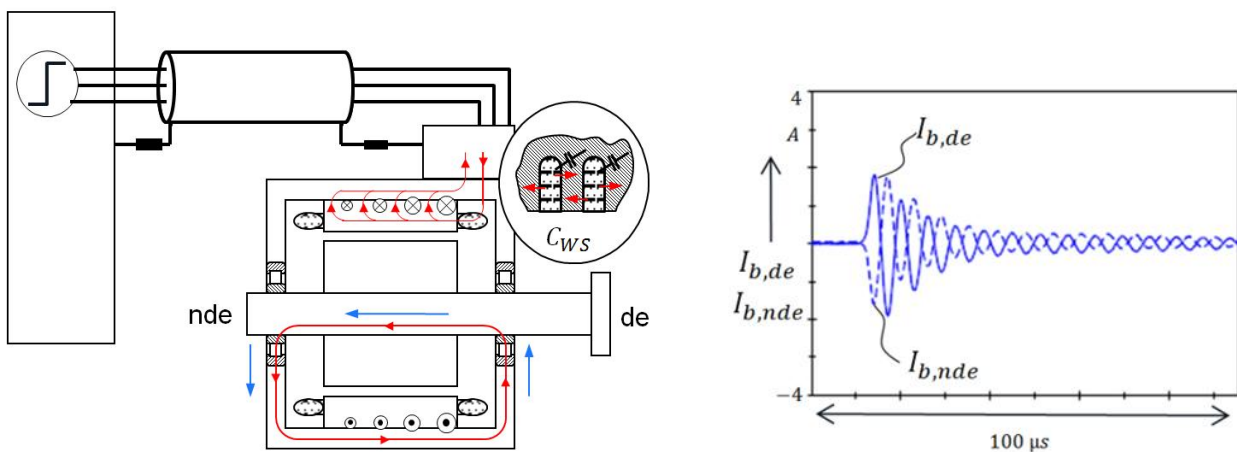


Figure 8 To the formation of circulating currents

An effective method to reduce the circular bearing currents is the installation of at least one bearing insulation. In Figure 9, two possible types of insulation are depicted. The left-hand side shows an arrangement with insulated bearing housing, the image on the right side shows the roller bearing with a ceramic-insulated outer ring.



46<sup>TH</sup> TURBOMACHINERY & 33<sup>RD</sup> PUMP SYMPOSIA  
HOUSTON, TEXAS | DECEMBER 11-14, 2017  
GEORGE R. BROWN CONVENTION CENTER

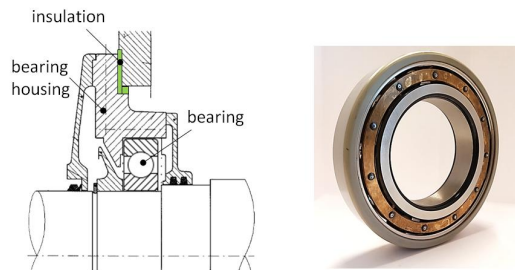


Figure 9 Different types of bearing insulations

### Rotor ground currents

The current flowing from the winding through the capacity  $C_{WS}$  - illustrated in Figure 5 - to the stator core lamination is routed back via the enclosing grounding system to the source – the DC link of the converter. In case, the grounding conditions at the motor are designed in such a way, that a path of low impedance is leading to the shaft of the motor, currents of considerable amplitude can flow via the connection motor shaft → coupling → load. In this way, they can potentially damage electrically passive plant component that are connected to the motor. Thus, the amplitude of the current from rotor to ground is strongly dependent on the quality of the enclosing grounding system. In Figure 10, the conditions are illustrated that are originated by the extension of the HF equivalent circuit diagram depicted in Figure 5. Here, the capacities of the motor, the load and the impedances of the enclosing grounding system can be identified.

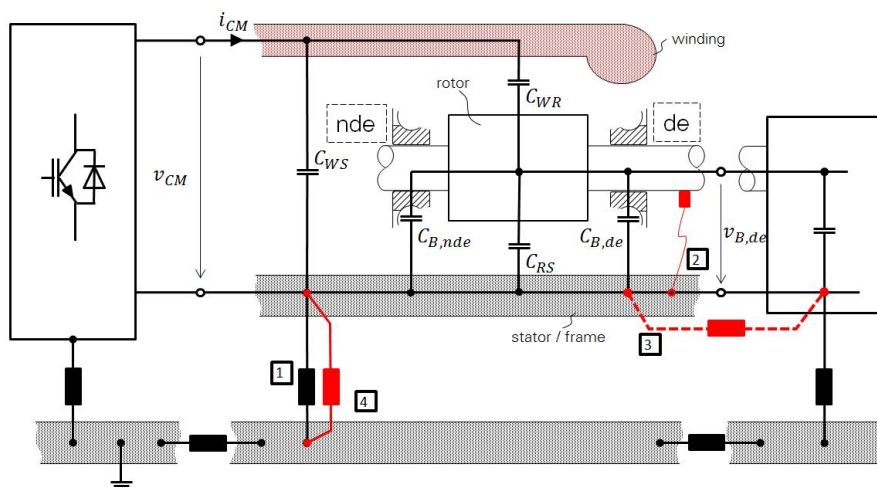


Figure 10 A motor integrated in a drive system

With regards to the possible rotor–ground current paths and their quality, the four cases depicted in Figure 11 have to be discriminated:

- (1) insufficient HF grounding of the motor (high impedance) and good HF-connection of the load (low impedance)  
→ current rotor–ground ↑↑, bearing NDE bearing ↑↑, current via the load ↑↑
- (2) like (1), but with additional grounding brush on the NDE side  
→ → current rotor–ground ↑↑, bearing NDE bearing ↓, current via the load ↑↑
- (3) like (1), but with additional equipotential bonding between motor and load  
→ → current rotor–ground ↓, bearing NDE bearing ↓, current via the load ↓
- (4) good HF grounding of the motor (low impedance) and good HF connection of the load (low impedance)  
→ current rotor–ground ↓↓, bearing NDE bearing ↓↓, current via the load ↓↓





46<sup>TH</sup> TURBOMACHINERY & 33<sup>RD</sup> PUMP SYMPOSIA  
 HOUSTON, TEXAS | DECEMBER 11-14, 2017  
 GEORGE R. BROWN CONVENTION CENTER

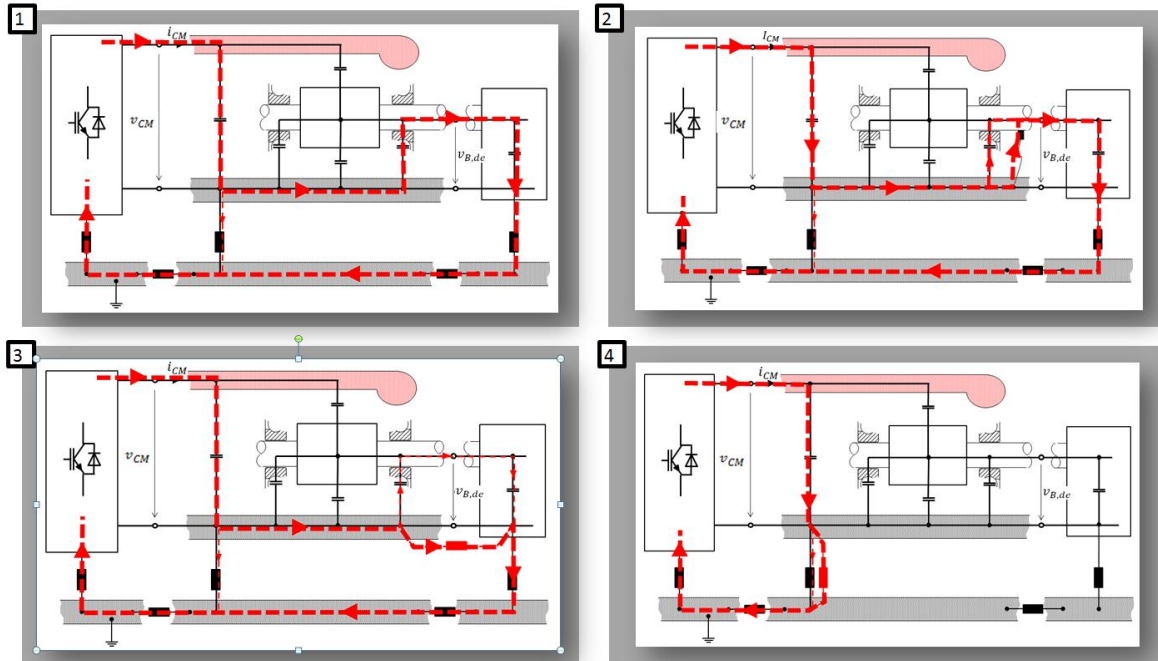


Figure 11 Possible rotor-ground current paths

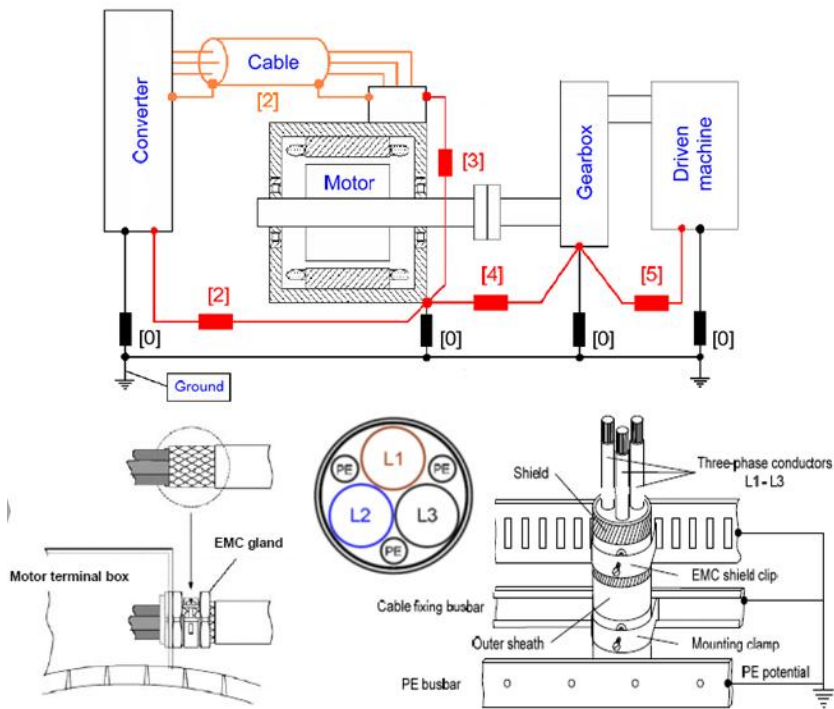


Figure 12 Possible measures to reduce rotor-ground currents



46<sup>TH</sup> TURBOMACHINERY & 33<sup>RD</sup> PUMP SYMPOSIA  
 HOUSTON, TEXAS | DECEMBER 11-14, 2017  
 GEORGE R. BROWN CONVENTION CENTER

One of the most important measures to reduce rotor–ground currents is the improvement of the impedance conditions [12]. The feasible measures are schematically shown in Figure 12. Summarized, these are:

- ⊕ HF grounding of the components (4)
- ⊕ Use symmetrically shielded motor connecting cables (4)
- ⊕ Potential bonding in the system (3)
- ⊕ Connection through the largest possible surface area (4)

Besides the improvement of the impedance conditions, another alternative would be, to install additional common mode inductivities (chokes), in order to reduce the excitation, i.e. the common mode current. [13, 14]. The attachment of nanocrystalline iron cores at the output of the inverter has proven to be a viable solution. For that, the iron cores have to be installed in all three phases (without ground), as shown in Figure 13- at the left. The effectiveness of these additional inductivities is exemplified in the form of measured curves of bearing currents and voltages in Figure 13- on the right side. One can see that the bearing currents are significantly reduced with increasing number of iron cores. The optimum number of iron cores is depending on the selected type of cable, the cable length and the motor power. The effectiveness of the iron cores is limited to high frequencies, i.e. low-frequency components in the common mode current will result in a magnetic saturation of the iron cores. These low-frequency components can arise e.g. from unsymmetrical motor cables or single conductor arrangements. Magnetic saturation can result in an almost complete neutralization of the effectiveness in the high-frequency range. With respect to the previously described EDM currents, the iron cores are not effective at all.

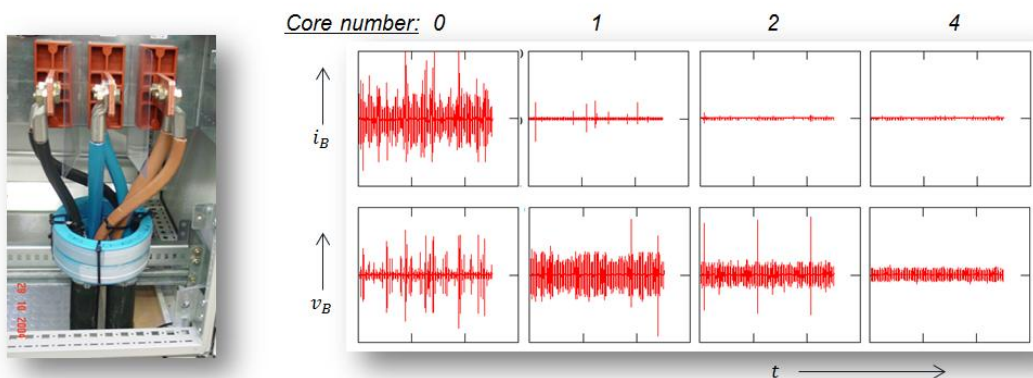
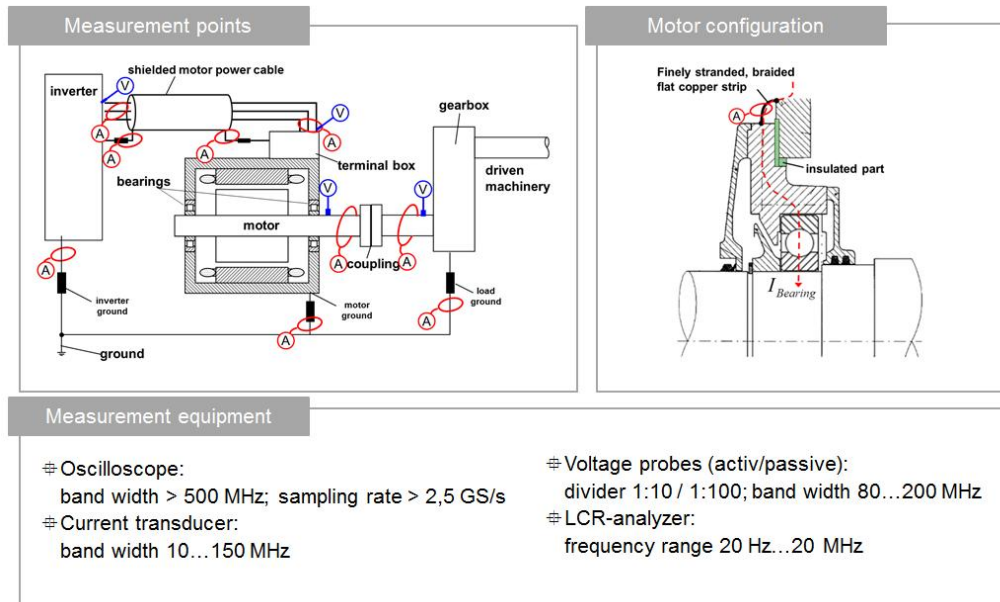


Figure 13 Application of nanocrystalline iron cores at the converter output

## ELECTRICAL BEARING CURRENT MEASUREMENTS

Bearing current measurements are an important tool to identify an adequate countermeasure to reduce the different types of stray currents. The motor is embedded in the total system that comprises converter, motor cable and system grounding. The corresponding parasitic leakage currents are the result of the interaction between all of the components. These currents can flow through the bearings of the drive units. The current which flows through a motor bearing cannot be directly measured. Suitable measures to reduce the current should be defined with a precise knowledge of the surrounding system quantities, which are of decisive significance. For plants and systems that are already operational, it is only possible to balance the ground currents flowing in and those flowing out [12]. It is not always possible to measure terminal and shaft voltages [8] (Figure 14, left). Bearing currents can be indirectly measured according to [1] within the scope of prototype and system tests in the motor laboratory. In this case, by locating and at the same time by bridging (using a jumper) an additional insulation layer in the area around the motor bearing, the current is measured, which also flows through the bearings connected in series. The jumper must have a low impedance at high frequencies and the insulation layer must have a low capacitance so that the bearing currents really do flow through the jumper and the amplitude is not erroneous (Figure 14, right). In systems that have already been implemented, this measurement type can only be used in the minority of cases. In order to perform the measurements, it is required to employ equipment that is suitable for the measurement of high-frequency signal amplitudes. These are oscilloscopes, current transformers and voltage probes with the appropriate sensitivity and bandwidth. A corresponding table together with the specification of the limits to be complied with, can be found in Figure 14 at the bottom.



**Figure 14** The most important external points for system measurements (left), the indirect bearing current measurement using supplementary insulation at the bearing (right) and the suitable equipment

An assessment of measurements of bearing currents according to Figure 14 at the right is indeed possible using different threshold approaches, nevertheless, due to frequently missing data, it is mostly difficult or impossible. As already mentioned previously, the measuring set up, as shown in the picture on the right, is a matter of a special version that normally only will be employed within the context of test runs in test benches. In Figure 15, possible valuation methods with the correspondent thresholds are depicted. The individual approaches can be summarized as follows:

⊕ Bearing current density [2, 15]

The quotient of the peak value of the measured bearing current and the Hertzian contact surface inside the bearing is referred to as apparent bearing current density. According to [2, 15], an assessment by the comparison with three result areas at current densities is feasible. Here, the distinction is made between an uncritical operation at current densities of  $< 0,3 \text{ A/mm}^2$  and a critical operation at values of  $> 0,8 \text{ A/mm}^2$  as well as a transition zone. In addition to the difficulty to capture the bearing current, the Hertzian contact surface is hard to calculate in real operation. Normally, the bearing loads, temperatures and speeds required for this, are not known so that the bearing current density can only be calculated in very rare cases. Furthermore, an unambiguous correlation to the damage could not be verified in [2].

⊕ Discharge energy [8, 16]

With the knowledge of the time courses of bearing current and bearing voltage, the discharge energy can be calculated according [8] from the integral of the product of these two parameters. This electrical energy of the arc discharge causes – depending on the magnitude – a melting or evaporation of the raceway material in the roller bearing. The latter is the trigger for the critical ripple formation. According to [8], a plausible limited value of approx.  $1 \mu\text{Ws}$  with associated vaporization craters of approx.  $4 \mu\text{m}$  can be estimated. The measurement of the time courses required for that, is usually impossible during real motor operation. That means, this limit value approach will more likely be applied within the context of defined test bench runs. Validated results proving their correlation with damages are currently not available.

⊕ Bearing apparent power [10]

According to [10], it is possible to calculate some kind of “apparent bearing power“ only with the aid of the product of the peak values of the two parameters bearing current and bearing voltage – without information about their time courses. This allows an estimated calculation of the electrical bearing load. The limit values captured in the context of test bench runs discriminate between uncritical operation at apparent powers of  $< 20 \text{ VA}$  and critical operation at values of  $> 60 \text{ VA}$  as well as an intermediate transition area.

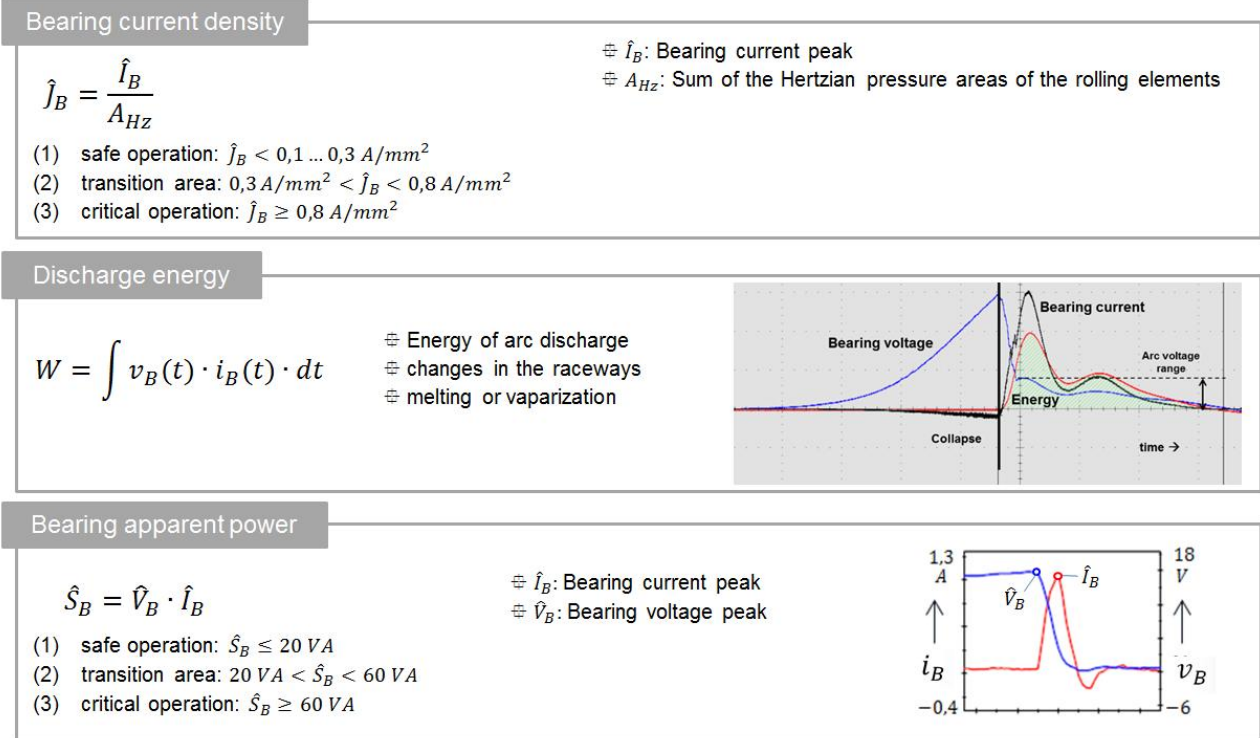


**Figure 15** Possible limits for safe bearing operation according to the literature

The measuring setup depicted in Figure 14 at the left is mainly used either completely or partially for system measurements in the field. Due to the fact that the amplitude of the bearing currents cannot be evaluated with this setup, the only way to achieve qualitative statements regarding the real bearing stress, is the evaluation of the external measured variables. However, in case of modifications of the electrical setup of the drive system, the effectiveness of measures can be rated by a relative comparison. A procedure describing the measuring process and the validation is shown in the summary of this paper.

A new approach for a sensor system for the assessment of bearing currents is outlined in [8, 17]. The basis is a detailed analysis of the voltage across the motor bearings. This can be used to indirectly estimate the bearing currents. A spark discharge within the bearing lubricant film is closely related to a corresponding steep voltage change. There is a direct relationship between the voltage change and the bearing current that flows. With this approach, it is possible to analyze the voltage breakdowns at the bearing and subsequently classify them. Motor-related sensor data is sent via a wireless link to a condition monitoring system. This generates a frequency distribution of the bearing current pulses that were detected. The schematic sensor structure is shown in Figure 16. A histogram of a typical frequency distribution with a large number of qualitative high bearing current impulses that occur in a certain time period is presented in the upper right picture; the lower the current impulses, the less critical the bearing condition.

The photos of a drive motor in the upper megawatt range during the system test and in real on-site operation are shown as an example. While the photo at the lower left shows the sophisticated system measurement with the aid of five oscilloscopes and the corresponding 20 measured points, the picture on the right represents the real plant operation, in which only the bearing current sensor provides the required statements regarding electrical bearing stress.



46<sup>TH</sup> TURBOMACHINERY & 33<sup>RD</sup> PUMP SYMPOSIA  
HOUSTON, TEXAS | DECEMBER 11-14, 2017  
GEORGE R. BROWN CONVENTION CENTER

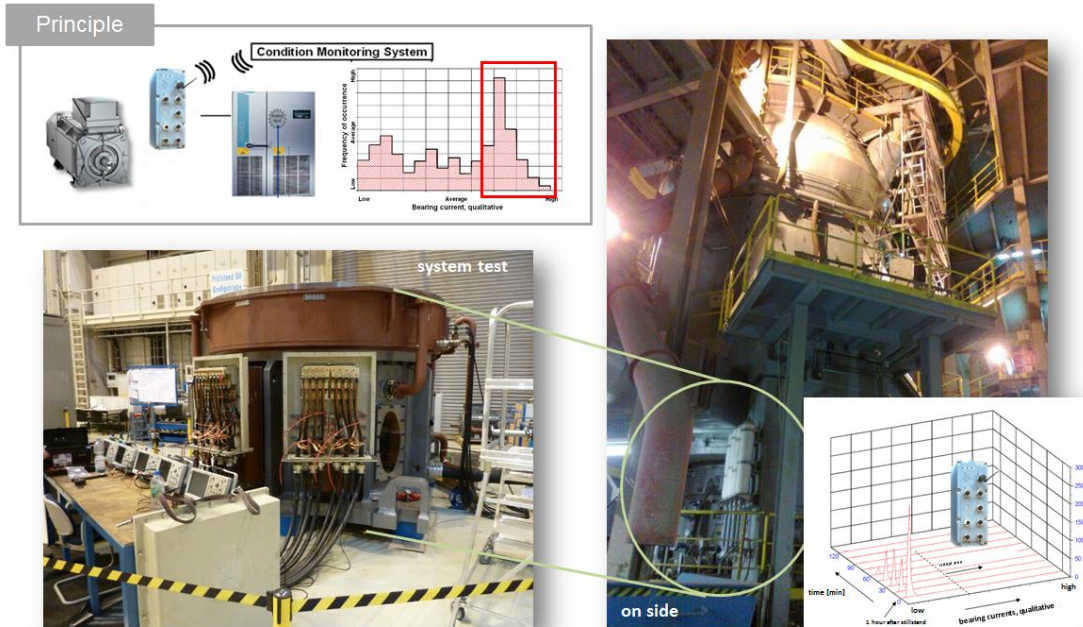


Figure 16 The bearing current sensor in system test and real on-site operation

## DETERMINATION OF THE MECHANICAL BEARING CONDITION

The assessment of electrical stress of the bearing is only one part of the bearing condition monitoring. With this approach it is possible to identify a potential danger for bearing faults as a result of electrical currents. More precise information about the mechanical condition of the bearing can be achieved via vibration analysis. A measurement of the vibration acceleration and the vibration velocity and the analysis of their time and frequency characteristics is an important tool to this direction. In addition to the RMS-values of the vibration acceleration and the vibration velocity as well as a specific broad band value, especially the frequency analysis by Fast Fourier Transform (FFT) and the envelope curve method are a well-known tools for detecting bearing damages [18–24].

### RMS-Value of the vibration acceleration

The RMS value of a vibration signal indicates the content and area of the time signal. As defined in [23], the RMS value refers to the vibration velocity signal in the frequency range 10 Hz to 1000 Hz. It is very suitable for the assessing of general machine vibrations (e.g. unbalance) in the frequency range up to 1 kHz. It is not suitable for detecting faults in rolling-contact bearings and gear units early on.

### $K(t)$ - value

A special kind of a broad band quantity is the  $K(t)$ -value. The relation is defined in [21, 24]. It is calculated from the root-mean-square and maximum absolute values of a broadband time signal of the vibratory acceleration. The ratio between the product of the current rootmean - square and maximum absolute values of the acceleration at the start ( $t = 0$ ) and at a suitable time is defined with following equation.

$$K(t) = \frac{a_{rms}(0) \cdot a_{peak}(0)}{a_{rms}(t) \cdot a_{peak}(t)} \quad (2)$$

Where  $a_{rms}$  is the RMS-value and  $a_{peak}$  the peak-value of the vibration acceleration for start ( $t = 0$ ) and  $t$ . By linking the peak and rms values of the acceleration signal the  $K(t)$  value indicates changes like “local pitting damages” (shock excitations) as well as raceway corrosion and flaking (distributed damages). For this different zones of degradation are defined in [24].



**46<sup>TH</sup> TURBOMACHINERY & 33<sup>RD</sup> PUMP SYMPOSIA**  
**HOUSTON, TEXAS | DECEMBER 11-14, 2017**  
**GEORGE R. BROWN CONVENTION CENTER**

**Table 1** K(t) Zones of degradation [24]

<b>Zone</b>	<b>K(t)</b>	<b>Degree of degradation</b>
①	1...0,5	Good running conditions
②	0,5...0,2	Ignition of degradation
③	0,2...0.02	Progressive degradation
④	<0,02	Damage

#### *FFT vibration acceleration*

The frequency-selective evaluation of vibration data allows you to determine the specific cause of a problem and localize the affected machine element. The time signals are broken down into their basic elements (according to Fourier's law). The different amplitudes for the associated frequencies are shown in the spectrum. This enables a qualitative assignment to the corresponding originators, which means that specific corrective measures can be planned. This method is not suitable for detecting early damage to rolling-contact bearings, however, because the extremely low-energy defect components from the rolling-contact bearings are hidden by the high-energy machine vibrations.

#### *Envelope analysis (curve)*

The envelope curve [18, 19] for assessing the condition of the bearing is obtained from the time signal for vibration acceleration. For machines in perfect working order, the envelope for this time signal is a straight, horizontal line. When the bearing moves over a damaged area, however, this triggers periodic force pulses that mask the machine vibrations and the straight, horizontal line is now periodically interrupted / masked by these pulses. The resulting envelope curve only contains information about the defect, which is why even the slightest defect can be detected, regardless of the high-energy machine vibrations that do not modulate the vibration signal in the frequency ranges analyzed. The time signal modulated by defect pulses can be demodulated by means of suitable filters, so the envelope curve is separated and subject to a frequency analysis. With suitably filtered time signals, only data relating to the damaged area where the bearing moves periodically over is displayed in the spectrum; stochastic components are explicitly suppressed. This method offers outstanding signal-to-noise characteristics and is, therefore, ideal for detecting damage early on.

### **COMPARISON OF DIFFERENT DETERMINATION METHODS**

A direct comparison between these analysis methods for the determination of the mechanical bearing status is only possible assuming unaltered constraints. In [25] a series of comparative studies on a bearing test bench, that has been specifically designed for that purpose, are presented. In doing so, besides the described mechanical analysis methods the presented bearing current sensor has been deployed.

#### *Bearing test stand measurements*

The bearing test stand shown in [8, 10] allows parameter tests to be performed with various relevant bearing types and sizes. In addition to the electrical operating parameters – such as bearing voltage and current – there are especially the mechanical parameters that can be changed separately. The range of the parameter settings is based on the field- and system test experience. Speed, temperature, load and vibration level at the test bearing can be adjusted – the last two regarding amplitude and frequency. An open-loop and closed-loop measuring control system allows closed-loop controlled operation where all of the relevant data can be simultaneously acquired. A schematic diagram of this test stand is shown in Figure 17. The test bearing is connected to the drive unit through the shaft and an insulated coupling. This allows any speed points and profiles to be set. A defined, steady-state radial load can be applied to the bearing system using a loading bearing. Dynamic load components are introduced into the system using an unbalance disk as well as an inertial shaker. The bearing temperature is kept at a constant value using heating cartridges.



46<sup>TH</sup> TURBOMACHINERY & 33<sup>RD</sup> PUMP SYMPOSIA  
HOUSTON, TEXAS | DECEMBER 11-14, 2017  
GEORGE R. BROWN CONVENTION CENTER

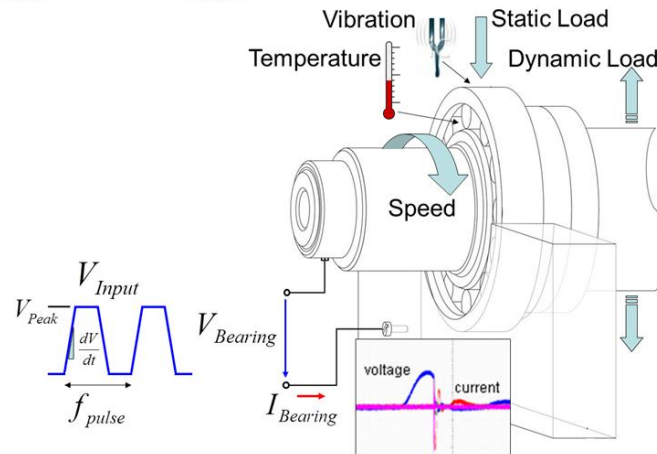


Figure 17 Bearing current test stand according to [8, 10]

In order to investigate the capability of the previously described bearing current sensor and the vibration analyzing methods to detect the presence of advancing bearing surface damage, i.e. corrugated patterns, an investigation with the following characteristics has been conducted: runtime = 600h, deep groove ball bearings (type 6210), BPO = 147Hz, BPI = 212 Hz, bearing load with unbalance disc at rotational speed = 36Hz and inertial shaker at 10Hz. The switching frequency of the voltage impulses applied on the bearing was set to 2.5 kHz. For this case the event rate of the actual discharge impulses, i.e. voltage collapses with subsequent current flow, was on average 75 impulses/second. The bearing voltage amplitudes were between 50 and 150V –the corresponding bearing current amplitudes in the range between 8 and 15 A, depending on the instant in time that the voltage collapses. The previously mentioned bearing voltage and current values indicate extremes, which should lead to an accelerated degradation of the bearing condition. The following electrical and mechanical measuring and analysis methods have been used in the test evaluation.

Table 2 Different measurement and analysis method used in the evaluation

Type	Method	Background
A	Bearing current sensor (BCS)	Measurement according to [8, 17]. Classification of the bearing current events according to the level and the frequency of occurrence.
B	FFT vibration acceleration	Frequency analysis of the vibration acceleration [18, 19]
C	Envelope analysis	Envelope analysis of the vibration acceleration [18, 19]
D	RMS-value	RMS-value of the vibration acceleration [20–23]
E	$K(t) - (1 / K(t))$	Calculated broad band value: $K(t)$ – Referring to [21, 24]

#### Selective frequency analysis

Figure 18 shows the FFT of the vertical vibration acceleration versus time for the 600 h parameter test. Over the runtime of the test different frequency components appeared. After 120 h multiples of the bypass frequency of the outer ring (BPO) occurred. This indicates an outer ring damage. After a runtime of 500 h frequency components with the bypass frequency of the inner ring (BPI) appeared. This indicates an inner ring damage. The same spectra are depicted in different diagrams for each time instant in Figure 19. Changes in the outer ring are detected after a time period of approx. 145h (t1, see also Figure 18), especially in the frequency range between 2 and 4 kHz, where distinct harmonic components at frequency intervals of 147 Hz emerge. After approx. 400h, the picture changes: harmonic components at frequency intervals of 212 Hz, corresponding to the inner race ball frequency (BPI), constitute the prominent peaks in the frequency spectrum at the frequency range between 1 and 1,8 kHz. The bearing damage is characterized by a transition from outer ring damage to a dominant inner ring damage. After approx. 550h (t2, see also Figure 18) the bearing damage can also be acoustically recognized. The corresponding pictures of the bearing raceways are shown in Figure 19. The different damage types of the inner and outer race of the test bearing can be clearly seen in these pictures.



46<sup>TH</sup> TURBOMACHINERY & 33<sup>RD</sup> PUMP SYMPOSIA  
 HOUSTON, TEXAS | DECEMBER 11-14, 2017  
 GEORGE R. BROWN CONVENTION CENTER

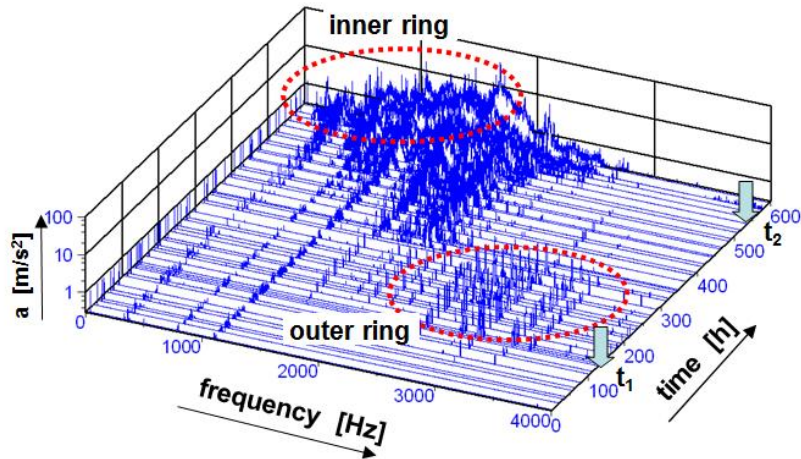


Figure 18 FFT of the vertical vibration acceleration versus time for the 600 h parameter test [17]

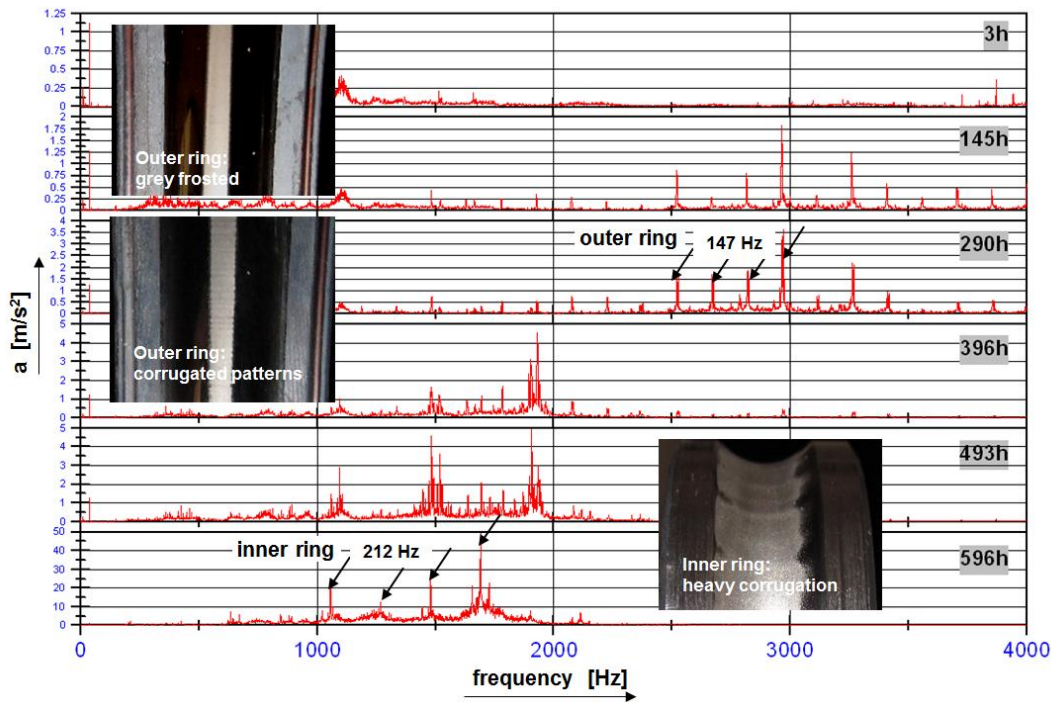


Figure 19 FFT of the vertical vibration acceleration at different time instants [17]

As described previously the envelope analyzing method offers outstanding signal-to-noise characteristics. Because of this the spectral components of the main bypass frequencies of the tested roller bearing can be displayed very clearly. In Figure 20 the envelope curves for two different time instants are shown. For the runtime of 150 h (outer ring corrugation grade 2-3) the BPO (147 Hz) and multiples of them are the main spectral lines. After 550 h (inner ring corrugation grade 4<sup>+</sup>) the BPI (212 Hz) and multiples can clearly be seen.



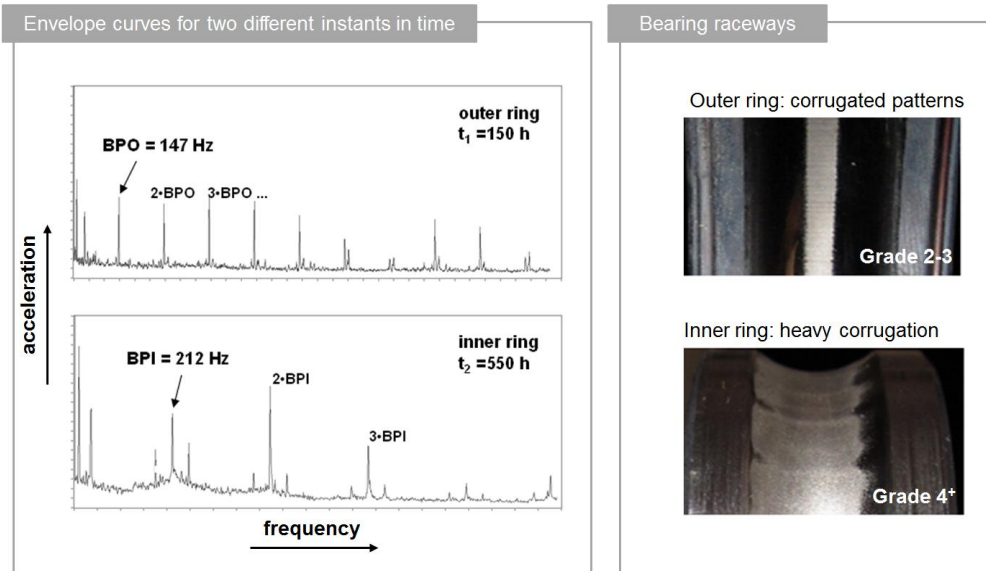


Figure 20 Envelope analysis for different instants of times [17]

#### Comparison and combination

The signatures of types A...C (Table 2) presented changes at a very early stage. This can be seen in the 3D-diagrams of Figure 18 for the FFT and in Figure 20 for the envelope analysis. In the FFT-analysis the harmonics located at the expected fault frequencies appear in the spectrum. By means of envelope analysis the characteristic fault frequencies for outer (BPO) and inner ring damage (BPI) can be identified (see Figure 19). In this case different faults occurred at different time instants. After 150 hours only the outer ring damage was visible with its characteristic damage frequency (BPO) of 147 Hz. After 350 hours an inner ring corrugation took additionally place with a fault frequency of 212 Hz (Figure 19). This inner ring damage increases very rapidly and is also much more extended compared to the damage of the outer ring. Therefore the characteristic fault peaks of the outer ring disappear in the FFT as well as in the envelope spectrum. By identifying the fault peaks and their frequencies it is possible to identify the fault location by the frequency of the corresponding harmonics and the fault severity by the corresponding amplitudes of these harmonics. In parallel to the increase of the mechanical bearing damage, the numbers of critical bearing current events measured by the bearing current sensor showed increased values. This fact can be explained by the higher number of bearing current events with increasing vibration level [8]. Thereby the formation of corrugated patterns increases via some kind of self-amplification process.

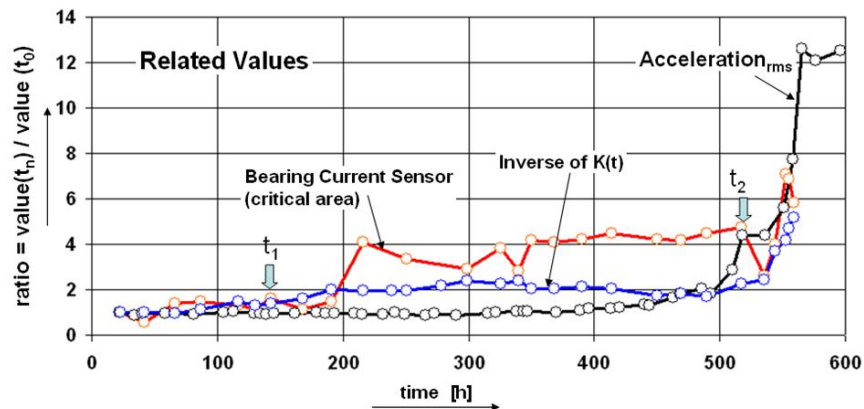


Figure 21 Comparison of the related values for different analysis methods [17]



46<sup>TH</sup> TURBOMACHINERY & 33<sup>RD</sup> PUMP SYMPOSIA  
 HOUSTON, TEXAS | DECEMBER 11-14, 2017  
 GEORGE R. BROWN CONVENTION CENTER

A comparison with the broad band signatures (type D, E in Table 2) shows that these methods are generally appropriate only to a limited extent or not at all for an early detection of electrically caused bearing damages. For a better comparison the related values of  $1/K(t)$  are displayed in the diagram of Figure 21. Only the bearing current sensor shows an increased number of events at the time when the outer ring damage appears.

Broadband measurements as shown above, have only little significance with regard to early detection of damages. Frequency-selective methods facilitate – besides localizing of the damage location – also the classification of the extent of damage. Especially the envelope curve technique is due to its very good signal-to-noise ratio an effective means to evaluate the mechanical bearing status during real plant operation. On the basis of empirical values out of a multitude of measurements on site, it is possible to define areas for the maximum amplitude of the spectral components of the vibration acceleration  $\hat{a}_{\text{Spek}}$ , which correspond to the levels of damage from ripple formation depicted in Figure 2. These values are summarized in the following table.

**Table 3** Assignment of the damage levels to the maximum amplitude of the spectral components of the vibration acceleration  $\hat{a}_{\text{Spek}}$  using the envelope curve analysis

Grade	$\hat{a}_{\text{Spek}}$ [m/s <sup>2</sup> ]
1	< 0,3
2	< 1,0
3	< 3,0
4	< 10
5	> 10

The listed Grade 5 in Table 3 corresponds to a bearing that exhibits fatigue failures in the raceways and at the balls in addition to the corrugation. This is adequate to a condition that can occur in the course of the far advanced damage process of ripple formation.

## CONCLUSIONS AND RECOMMENDATIONS

When operating electric motors in state-of-the-art drive systems a series of parasitic effects occur as a result of the fast-switching converters. One of these is the current that flows through the motor bearings. This current can be classified in at least three different ways: In high-frequency, circulating currents in the motor, EDM currents as arc discharges in the bearing lubricant gap, as well as high-frequency rotor-ground currents. The first type results from a circulating flux in the motor and can be significantly reduced by using at least one insulated motor bearing. The magnitude of the rotor-ground current strongly depends on the quality of the grounding system. Suitable measures, up to HF-capable systems significantly improve the situation. The so-called EDM currents result from the converter common-mode voltage. The shaft voltage of the motor is an image of this voltage and leads to a potential difference between the rotor and the stator of the motor. When the critical breakdown threshold in the bearing lubricant gap is exceeded, the subsequent arc discharge can melt or vaporize material in the bearing raceways and lead to the so called corrugated patterns. Detailed informations concerning a bearing damage due to corrugation caused by electrical currents through the bearing can only be drawn by a combined analysis of the electrical and the mechanical behavior of the bearing.

The electrical bearing load can only be measured indirectly. Due to the fact that during real plant operation complex analyses at specially prepared motors are usually not feasible, it is necessary to retrieve at least qualitative statements on the actual electrical bearing load by means of investigations in the overall system. Therewith, the direct transfer to the limit values presented in this paper (Figure 15) is not feasible, however, comparative results regarding the status can be derived. By means of measuring of the bearing voltage at the DE side of the motor and assessments on the voltage waveform, it is possible to narrow down the actual type of bearing current more precisely. In case of the voltage across motor the bearing has a step waveform in time domain, as depicted in Figure 7, the EDM currents are dominant. In other voltage waveform cases, the discrimination between circular and rotor-ground current by means of measuring the shaft current is feasible. As presented in detail in this document, possible remedies are the controlled utilization of grounding brushes (EDM currents), the installation of an insulated bearing on the NDE side of the motor (circular currents) and/or a modification of the grounding system by means of using shielded, symmetrical motor cables as well as equipotential bonding in the overall system. The common mode current flowing into the drive system and by that also the electrical bearing load can be reduced by accompanying employment of common mode chokes in the form of nanocrystalline iron cores.



46<sup>TH</sup> TURBOMACHINERY & 33<sup>RD</sup> PUMP SYMPOSIA  
 HOUSTON, TEXAS | DECEMBER 11-14, 2017  
 GEORGE R. BROWN CONVENTION CENTER

The precise evaluation of the mechanical bearing status is only possible by frequency-selective analysis methods. Particularly the early detection of corrugation can be achieved by applying the so-called envelope curve analysis on the basis of vibration acceleration values at the bearing location to be considered. All broadband values reveal alterations of the bearing status only very much delayed. The assessment of the current bearing condition can be performed by comparing the measuring values with those limit values given in Table 3 whether appropriate correlation to the actual damage level according to the possible grades of corrugations presented in Figure 2.

## NOMENCLATURE

### *Symbols*

$a_{\text{rms}}$	= RMS value of the vibration acceleration	[m/s <sup>2</sup> ]
$\hat{a}_{\text{spec}}$	= max. amplitude of the spectral component	[m/s <sup>2</sup> ]
$A_{\text{Hz}}$	= Hertz'ian pressure area	[mm <sup>2</sup> ]
BPO	= Bypass frequency of the bearing outer ring	[Hz]
BPI	= Bypass frequency of the bearing inner ring	[Hz]
$C_{\text{WS}}$	= Capacitance winding-stator	[nF]
$C_{\text{WR}}$	= Capacitance winding-rotor	[pF]
$C_{\text{RS}}$	= Capacitance rotor-stator	[pF]
$C_{\text{B}}$	= Capacitance bearing	[pF]
$f_{\text{S}}$	= Switching frequency of the converter	[kHz]
$i_{\text{CM}}$	= Common mode current	[A]
$i_{\text{B}}$	= Bearing current	[A]
$J_{\text{B}}$	= Bearing current density	[A/mm <sup>2</sup> ]
$K(t)$	= Vibration broad band quantity	
$S_{\text{B}}$	= Bearing apparent power	[VA]
$dv/dt$	= Steepness of the voltage change	[kV/ $\mu$ s]
$V_{\text{D}}$	= DC-link voltage	[V]
$v_{\text{RG}}$	= Phase to ground voltage phase R	[V]
$v_{\text{CM}}$	= Common mode voltage	[V]
$v_{\text{B}}$	= Bearing voltage	[V]
$W$	= Discharge energy	[ $\mu$ Ws]

### *Acronyms*

BCS	= Bearing current sensor
BVR	= Bearing voltage ratio
DE	= Drive end
EDM	= Electrostatic discharge machining
FFT	= Fast Fourier Transformation
HF	= High frequency
NDE	= Non drive end
SEM	= Scanning electron microscope
VSI	= Voltage source inverter



46<sup>TH</sup> TURBOMACHINERY & 33<sup>RD</sup> PUMP SYMPOSIA  
HOUSTON, TEXAS | DECEMBER 11-14, 2017  
GEORGE R. BROWN CONVENTION CENTER

## REFERENCES

- [1] V. Hausberg, *Elektrische Lagerbeanspruchung umrichter gespeister Induktionsmaschinen*. Univ., Diss.--Hannover, 2001. Düsseldorf: VDI-Verl., 2002.
- [2] A. Mütze, *Bearing currents in inverter fed AC-motors*. Diss., TU-Darmstadt. Aachen: Shaker, 2004.
- [3] J. M. Erdman, R. J. Kerkman, D. W. Schlegel, and G. L. Skibinski, "Effect of PWM inverters on AC motor bearing currents and shaft voltages," *Industry Applications, IEEE Transactions on*, vol. 32, no. 2, pp. 250–259, 1996.
- [4] Shaotang Chen and T. A. Lipo, "Bearing currents and shaft voltages of an induction motor under hard- and soft-switching inverter excitation," *IEEE Trans. on Ind. Applicat.*, vol. 34, no. 5, pp. 1042–1048, 1998.
- [5] S. Chen, T. A. Lipo, and D. Fitzgerald, "Source of induction motor bearing currents caused by PWM inverters," *IEEE Trans. On energy Conversion*, vol. 11, no. 1, pp. 25–32, 1996.
- [6] A. Binder, R. Aust, and A. Schrepfer, "Bearing currents - a danger to inverter-fed a-c motors?," *Iron and Steel Engineer*, vol. 76, no. 7, pp. 47–52, 1999.
- [7] A. Muetze, "On a New Type of Inverter-Induced Bearing Current in Large Drives With One Journal Bearing," *Industry Applications, IEEE Transactions on*, vol. 46, no. 1, pp. 240–248, 2010.
- [8] H. Tischmacher and S. Gattermann, "Bearing currents in converter operation," in *Electrical Machines (ICEM), 2010 XIX International Conference on*, 2010, pp. 1–8.
- [9] H. Tischmacher and O. Kartashov, "Simulation von Lichtbogenentladungen in Wälzlagern von Elektromotoren zur Interpretation von experimentellen Ergebnissen an einem Lagerversuchsstand," in *ANSYS Conference 2014*, pp. 1–12.
- [10] H. Tischmacher, *Systemanalysen zur elektrischen Belastung von Wälzlagern bei umrichter gespeisten Elektromotoren*. Univ., Diss., Hannover 2017, Veröffentlichung in 2017.
- [11] Alger and Samson, "Shaft currents in electric machines," *A.I.E.E., Journal of the*, vol. 43, no. 11, pp. 1081–1082, 1924.
- [12] P. J. Link, "Minimizing electric bearing currents in adjustable speed drive systems," in *Conference Record of 1998 Annual Pulp and Paper Industry Technical Conference*, Jun. 1998, pp. 181–195.
- [13] A. Muetze, "Scaling Issues for Common-Mode Chokes to Mitigate Ground Currents in Inverter-Based Drive Systems," *Industry Applications, IEEE Transactions on*, vol. 45, no. 1, pp. 286–294, 2009.
- [14] A. Muetze and Bee See Heng, "Performance of Common-Mode Chokes," *Industry Applications Magazine, IEEE*, vol. 16, no. 2, pp. 31–38, 2010.
- [15] D. Busse, J. Erdman, R. J. Kerkman, D. Schlegel, and G. Skibinski, "Bearing currents and their relationship to PWM drives," *Power Electronics, IEEE Transactions on*, vol. 12, no. 2, pp. 243–252, 1997.
- [16] T. Zika, "Electric discharge damaging in lubricated rolling contacts," TU Wien, 2010.
- [17] H. Tischmacher and S. Gattermann, "Bearing Current Measurement System for Drive Systems," in *International Symposium on Electromagnetic Fields in Mechatronics, Electrical and Electronic Engineering*, 2011.
- [18] Y.-T. Sheen, "An envelope analysis based on the resonance modes of the mechanical system for the bearing defect diagnosis," *Measurement*, vol. vol. 43, no. issue 7, pp. 912–934, 2010.
- [19] A. Sturm and S. Billhardt, "Envelope curve analysis of machines with rolling-element bearings," in *Fault Detection Supervision and Safety for Technical Processes (SAFEPROCESS '91)*, 1991.
- [20] A. Piccirelli, "Development of an expert system for diagnosis of mechanical wear of a machinery park in steel industry: (in german)," *Technical Steel Research Series*, pp. 1–44, 1998.
- [21] *VDI 3832: Measurement of structure-borne sound of rolling element bearings in machines and plants for evaluation of condition*, VDI 3832, 2013.
- [22] *DIN ISO 10816-1: Mechanische Schwingungen - Bewertung der Schwingungen von Maschinen durch Messungen an nicht-rotierenden Teilen - Teil 1: Allgemeine Anleitungen (ISO 10816-1:1995)*, DIN ISO 10816-1, 1997.
- [23] *DIN ISO 10816-3: Mechanische Schwingungen - Bewertung der Schwingungen von Maschinen durch Messungen an nicht-rotierenden Teilen - Teil 3: Industrielle Maschinen mit einer Nennleistung über 15 kW und Nenndrehzahlen zwischen 120 min-1 und 15000 min-1 bei Messungen am Aufstellungsort (ISO 10816-3:2009)*, DIN ISO 10816-3, 2009.
- [24] A. Sturm, R. Foerster, and N. Hippmann, *Waelzlagendiagnose an Maschinen und Anlagen*: TUEV Rheinland, 1986.
- [25] H. Tischmacher and S. Gattermann, "Multiple signature analysis for the detection of bearing currents and the assessment of the resulting bearing wear," in *Power Electronics, Electrical Drives, Automation and Motion (SPEEDAM), 2012 International Symposium on*, 2012, pp. 1354–1359.